TẠP CHÍ KHOA HỌC
TRƯỜNG ĐẠI HỌC QUY NHƠN

Cấu trúc và tính chất quang của vật liệu zirconium(oxy)nitride tổng hợp từ hạt nano zirconium dioxide

Nguyễn Thị Minh Uyên[1], Lê Trần Phương Thảo[1], Đặng Bùi Nhật Lê[2], Lê Thị Mỹ Nhi[3], Phạm Quỳnh Nhi[3], Lê Thị Bích Tuyền[3], Văn Thị Thùy Trang[1], Lê Thị Ngọc Loan[1,*]

[1]Khoa Khoa học Tự nhiên, Trường Đại học Quy Nhơn, Việt Nam
[2]Khoa Khoa học và kỹ thuật vật liệu, Trường Đại học Phenikaa, Việt Nam
[3]Khoa Sư phạm, Trường Đại học Quy Nhơn, Việt Nam

Ngày nhận bài: 16/08/2023; Ngày sửa bài: 06/10/2023; Ngày nhận đăng: 13/10/2023; Ngày xuất bản: 28/10/2023

TÓM TẮT

Trong những năm gần đây, việc sử dụng thiết bị thu nhiệt năng mặt trời đang ngày càng gia tăng vì đây là một phương pháp trực tiếp và hiệu quả để biến năng lượng mặt trời thành các nguồn năng lượng có thể sử dụng được. Trong xu hướng này, các nghiên cứu tập trung vào việc phát triển cấu trúc nano của các nitride kim loại chuyển tiếp và oxynitride kim loại, nhằm tối đa hóa khả năng thu năng lượng từ mặt trời. Trong nghiên cứu này, vật liệu zirconium(oxy)nitride (Zr(O)N) đã được tổng hợp thành công bằng cách xử lý ZrO_2 trong môi trường khí NH_3 ở nhiệt độ cao nhằm ứng dụng trong quá trình chuyển đổi năng lượng quang nhiệt. Để xác định đặc điểm cấu trúc tinh thể, hình thái và tính chất của các vật liệu này, các kỹ thuật phân tích như nhiễu xạ tia X (XRD), kính hiển vi điện tử quét (SEM) và phân tích phổ phản xạ khuếch tán tử ngoại khả kiến (UV-Vis DRS) đã được sử dụng. Các kết quả cho thấy rằng pha tinh thể zirconium(oxy)nitride bắt đầu hình thành ở nhiệt độ 1150 ^oC. Các vật liệu Zr(O)N đã tổng hợp thể hiện khả năng hấp thụ năng lượng mặt trời và tạo ra nhiệt một cách hiệu quả. Các kết quả này cho thấy Zr(O)N có thể được tổng hợp bằng phương pháp đơn giản và có tiềm năng lớn trong các ứng dụng chuyển hóa năng lượng quang - nhiệt.

Từ khóa: *Hạt nano ZrO_2, ZrN, Zr(O)N, chuyển hóa năng lượng quang nhiệt.*

**Tác giả liên hệ chính.*
Email: lethingocloan@qnu.edu.vn

https://doi.org/10.52111/qnjs.2023.17509

QUY NHON UNIVERSITY
JOURNAL OF SCIENCE

Structural and optical characterization of zirconium(oxy)nitride synthesized from zirconium dioxide nanoparticles

Nguyen Thi Minh Uyen[1], Le Tran Phuong Thao[1], Dang Bui Nhat Le[2], Le Thi My Nhi[3], Pham Quynh Nhi[3], Le Thi Bich Tuyen[3], Van Thi Thuy Trang[1], Le Thi Ngoc Loan[1,*]

[1]Faculty of Natural Sciences, Quy Nhon University, Vietnam
[2]Faculty of Materials Science and Engineering, Phenikaa University, Vietnam
[3]Faculty of Pedagogy, Quy Nhon University, Vietnam

Received: 16/08/2023; Revised: 06/10/2023; Accepted: 13/10/2023; Published: 28/10/2023

ABSTRACT

In recent years, there has been a growing focus on solar thermal collectors as they offer a direct and efficient means of converting solar energy into usable forms. In line with this, significant attention has been directed towards advancing transition metal nitride and metal oxynitride nanostructures for solar-thermal collectors to maximize solar energy harvesting. In this study, we have successfully synthesized zirconium(oxy)nitride (Zr(O)N) materials for photothermal energy conversion. The process involved treating ZrO_2 in NH_3 at high temperatures, resulting in the creation of nanoparticles with promising properties. To characterize the materials, we conducted thorough investigations using X-ray diffraction (XRD), scanning electron microscopy (SEM), and ultraviolet-visible diffuse reflectance spectroscopy (UV-Vis DRS). The findings indicate that the Zr(O)N crystalline phase initiates its formation at 1150 °C. The Zr(O)N materials possess a robust capacity for absorbing solar energy and efficiently producing heat. Furthermore, these outcomes highlight the feasibility of synthesizing Zr(O)N through a straightforward approach, underscoring their significant potential for applications in photothermal conversion.

Keywords: *ZrO_2 nanoparticles, ZrN, Zr(O)N, photothermal energy conversion.*

1. INTRODUCTION

In recent times, there has been a notable increase in the exploration of group IVB transition-metal nitrides, as opposed to noble metals like Au and Ag, to broaden the scope of plasmonic applications and deepen our understanding of light-matter interactions.[1,2] This shift has the potential to revolutionize core technologies in fields such as telecommunications, computing, efficient solar harvesting, solid-state lighting, photochemistry, photo- and bio-sensing, diagnostics, and therapeutics.[3,4] Among these materials, titanium nitride (TiN) has garnered significant interest. However, zirconium nitride (ZrN) holds particular importance due to its distinct physical properties, including excellent anti-corrosion characteristics and a high melting point.[5] Importantly, ZrN exhibits a zero crossover wavelength within the visible spectrum, similar to Au, which grants them plasmonic properties in the visible and near-infrared regions.[3] This

**Corresponding author.*
Email: lethingocloan@qnu.edu.vn

https://doi.org/10.52111/qnjs.2023.17509

feature enhances their ability to absorb sunlight and convert it into heat, making them highly suitable for solar light harvesting applications.[6]

Numerous techniques can be employed for the synthesis of ZrN, such as high-energy ball milling of Zr elemental powders in a nitrogen gas environment at room temperature,[7] the magnesium thermal reduction process,[8] a nonthermal plasma reactor,[9] the initiation of exothermal reactions through microwave radiation,[10] and the utilization of metalorganic chemical vapor deposition method.[11,12] Among these approaches, the reduction-nitridation of zirconium oxide (ZrO_2) is frequently employed for the synthesis of zirconium nitride. This method involves the direct nitriding of ZrO_2 using ammonia gas at elevated temperatures.[12-14]

Zirconium Nitride (ZrN) possesses distinctive properties, including a high melting point (2952 ^oC) and single crystal hardness (22.7±1.7 GPa), strong covalent Zr-N bonding and excellent chemical resistance, and stability, making it highly suitable for applications as coatings and protective layers.[15-17] Recently, ZrN has garnered attention as an excellent material for electrodes in energy storage and conversion,[18] owing to its exceptional electrical conductivity, mobility, and impressive electrochemical performance.[4,19,20] Moreover, ZrN has emerged as a promising alternative plasmonic material, finding diverse applications in solar cells,[21] solar light harvesting,[22] and solar to heat energy conversion.[23,24] Its unique properties make it a valuable candidate in these solar-related technologies. Furthermore, zirconium oxynitride, similar to zirconium nitride, has piqued special interest as a material for solar-thermal collectors. This interest is due to its remarkable solar absorptance and thermal stability.[9,24,25] Thus, both ZrN and zirconium oxynitride exhibit great potential in advancing various applications related to energy conversion and utilization.

In this study, a straightforward approach was introduced to produce zirconium(oxy)nitride nanoparticles through the reduction-nitridation process of zirconium oxide nanoparticles (ZrO_2 NPs) in NH_3 gas at elevated temperatures. SEM images illustrated that average particles increased during nitridation process. Notably, the results revealed the formation of cubic ZrN phase at 1150 °C, and the materials exhibited strong and broad absorption spanning from the visible to near-infrared region (~300 – 2000 nm). Furthermore, the potential of the synthesized nanoparticles in solar-thermal energy conversion was also assessed.

2. EXPERIMENTAL

2.1. Chemicals

The raw materials used in this study including zirconium dioxide (ZrO_2, 99.95%), zirconium nitride (ZrN, 99.9%), ammonia and nitrogen gas (NH_3, H_2, > 99.9%) were supplied from Aladdin Reagent Co., Ltd., China.

2.2. NH_3 treatment of ZrO_2 nano particles

Initially, 8 mg of ZrO_2 powder was carefully placed into a ceramic boat, which was then positioned at the center of a quartz-tube furnace using a customized setup. This setup allowed for precise control of temperature, pressure, and gas flow during the experiment. One end of the quartz tube was connected to the gas inlet, with N_2 and NH_3 gases available. The other end was connected to a mechanical vacuum pump. To begin the process, the quartz tube was evacuated to achieve a vacuum level of 10^{-3} mbar. Subsequently, the furnace was pre-heated to 300 °C. To eliminate any contaminants, the tube was purged multiple times with N_2 gas. Once prepared, the temperature in the furnace was raised either to 1050 or 1150 °C, both at a ramping rate of 5 °C min^{-1}. After the desired temperature was stabilized, pure ammonia gas was continuously introduced into the furnace at a flow rate of 400 sccm for a duration of

1.5 hours. Following this, the furnace was gradually cooled down to 100 °C in an NH_3 environment and further to room temperature in N_2 before unloading the sample.

2.3. Material characterization

The crystalline structure of the obtained samples was studied by powder X-ray diffraction (XRD) employing an X-ray diffractometer (Brucker Phaser, D2) using Cu Kα irradiation (λ = 0.154 nm). The surface morphology of the synthesized materials was characterized by scanning electron microscopy (SEM) using a HITACHI S-4800 microscope. UV-Vis absorption spectra were measured using a Shimadzu 2600 UV-visible spectrometer.

2.4. Photothermal materials study

For each experimental run, 0.8g of PVP (Polyvinylpyrrolidone) and 9.5 mL of DMF (N,N-Dimethylformamide) were combined in a 100 mL glass beaker and stirred for a period of 4 hours. Subsequently, 0.01g of ZrO_2 1150 nanoparticles was added to the mixture and dispersed with sonication for 10 minutes. The resulting ZrO_2 1150 nanoparticle suspension was then used to create thin layers on glass slides (2 cm x 2 cm) through the spin-coating method, spinning at 1500 rpm for 60 seconds.

To evaluate the solar-thermal energy conversion performance of the prepared samples, a custom-made closed metal chamber made of steel was utilized. The metal chamber was insulated with fiber glass material to minimize heat loss. The prepared samples were placed at the center of this chamber and exposed to sunlight irradiation. The temperature of the ZrO_2 1150 layer was monitored using a K-type temperature probe. Additionally, temperature measurements inside the chamber and the ambient air outside were recorded using mercury temperature meters. The photon flux of sunlight was measured using a luminous flux meter from China. Throughout the experiments, data was recorded at 10-minute intervals to analyze the performance of the samples.

3. RESULTS AND DISCUSSION

The XRD patterns of the ZrO_2 NPs before and after the NH_3 treatment at 1050 and 1150 °C (sample ZrO_2 1050 and ZrO_2 1150) are presented in Figure 1. In the case of ZrO_2 nanoparticles (referred to as ZrO_2 TM), all observed diffraction peaks corresponding to monoclinic (m) and tetragonal (t) crystal structure phases were accurately matched with standard data of ZrO_2 (PDF Card - 00-036-0420 and PDF Card - 00-042-1164, respectively).[26,27] This result also indicates high purity of ZrO_2 TM (red trace).

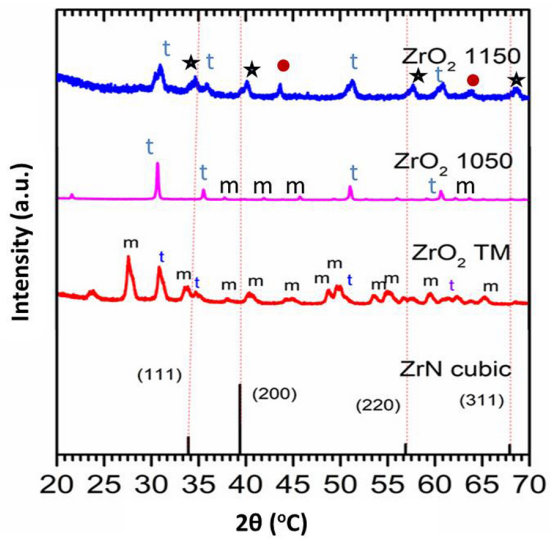

Figure 1. XRD diffraction patterns of ZrO_2 precusor and ZrO_2 after annealing in NH_3 at 1050 and 1150 °C.

Upon NH_3 treatment of ZrO_2 at 1050 °C, the peaks related to the monoclinic (m) phase of ZrO_2 nearly vanish, while most of those corresponding to the tetragonal ZrO_2 remain, e.g., at 31.3°, 36.3°, 52.3° and 62.1° (pink trace).[28,29] Furthermore, at the higher temperature of 1150 °C, the treatment results in the appearance of new peaks at 33.9°, 39.4°, 56.9°, and 67.9° (black stars), corresponding to diffraction planes of the (111), (200), (220), and (311) atomic planes of the face-centered cubic (FCC) structure of ZrN (PDF Card - 00-031-1493).[16,30] There are two peaks at 43.1° and 63.2° (red dots) which can be attributed to the insulating-metallic phase transition (ZrO_xN_y).[29]

https://doi.org/10.52111/qnjs.2023.17509

Interestingly, annealing ZrO_2 in NH_3 transforms the mixture of monoclinic and tetragonal crystal structure phases into the single phase of t-ZrO_2 and initiates a new phase of ZrN.

Figure 2 displays scanning electron microscopy (SEM) images of a representative sample, along with the particle size distribution, which was measured and determined using Digital Micrograph.

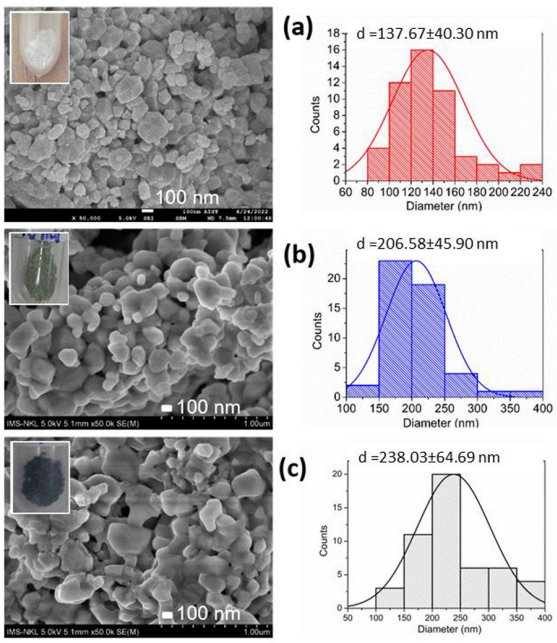

Figure 2. SEM images and the particle size distribution of (a) ZrO_2 TM, as well as ZrO_2 after being treated in NH_3 at different temperatures: (b) 1050 °C, and (c) 1150 °C. The color of the powders is also illustrated in the respective insets.

The SEM images present the shapes and sizes of ZrO_2 TM nanoparticles (Figure 2a) and the same nanoparticles after annealing in ammonia at 1050 °C (Fig. 2b) and 1150 °C (Figure 2c). In Figure 2a, ZrO_2 TM exhibits a wide variation in particle sizes, with an average diameter of approximately 137.67 ± 40.30 nm, represented by the top red distribution curve. After treatment at 1050 °C, the average diameter increases significantly to 206.58 ± 45.90 nm, a nearly 15% increment, as shown by the middle blue distribution. Subsequently, the particle size further grows by about 17% after treatment NH_3 at 1150 °C, resulting in an average diameter of about 238.03 ± 64.69 nm, as illustrated in the bottom black curve. The growth of particle sizes is due to higher reaction temperature. In addition, the substantial differences in size between the ZrO_2 1050 and ZrO_2 1150 samples, approximately 22% and 27%, respectively, can be attributed to the significant variability in the size of the ZrO_2 TM particles, estimated to be around 29%.

The findings reveal that NH_3 treatment at temperatures ranging from 1050 to 1150 °C does not significantly impact the surface morphology of the nanoparticles. However, it does induce remarkable changes in both particle size and the appearance of the powder color. These color variations are clearly visible in the optical images within the SEM images, showcasing a gradual shift from white (ZrO_2 TM) to dark gray (ZrO_2 1050) and ultimately black (ZrO_2 1150), which is the typical color of ZrN powder. This color transformation aligns with the light absorption characteristics observed in the following UV-Vis absorption spectra.

To investigate the optical properties of the composites, UV-vis diffuse reflectance spectral analysis was conducted on ZrO_2 powder, as well as the ZrO_2 samples treated in NH_3 at 1050 and 1150 °C. The results obtained from the analysis are presented in Figure 3.

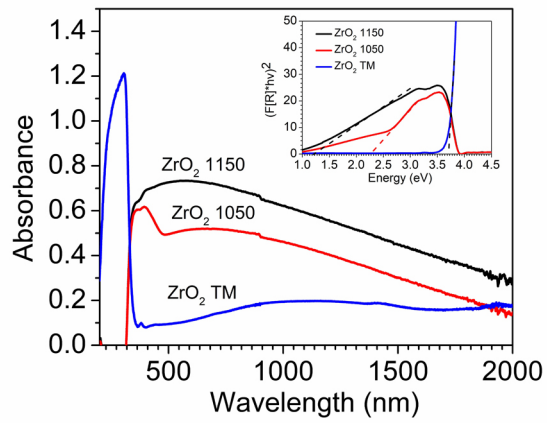

Figure 3. UV-Vis absorption spectra of the representative samples and the corresponding band gap calculations using the Kubelka-Munk method as indicated in the inset.

The UV-Vis absorption spectrum ZrO_2 TM shows a sharp and prominent absorption band with maximum at around 277 nm (4.48 eV in photon energy) which can arise due to the transition between valence band to conduction band.[28,31] However, this absorption peak for the ZrO_2 nanostructure in the UV-region is at lower energy as compared to the previous report on the optical band gap for bulk ZrO_2 (5.0 eV).[32] This indicates that there is still contribution from extrinsic states towards the absorption in this region. Apart from the strong absorption peak, a broad and weak absorption from visible to near infrared exists. The weak absorption in the visible and near IR region is expected to arise from transitions involving extrinsic states such as surface trap states or defect states or impurities.[32] The direct band gap energy can be determined by Kubelka-Munk method, about 3.7 eV, as indicated by the blue trace in the inset of Figure 3.

When comparing with pure ZrO_2, the absorption spectrum of ZrO_2 1050 reveals distinct characteristics. It displays a pronounced absorption peak at 391 nm with an energy gap (E_g) of approximately 2.3 eV, as depicted in the red trace within the inset. Additionally, there is a broad and potent absorption band spanning from the visible to the near-infrared spectrum. The initial absorption can be attributed to the band gap of zirconium oxynitride,[28,33,34] while the broad absorption is the result of a continuous depopulation of the d-band and the creation of an energy gap between the valence band and the Fermi level.[35]

Upon increasing the annealing temperature to 1150 °C, a phase transition to ZrN commences from the outer layer of ZrO_2 1150 particles, as evidenced by the XRD pattern. This transformation yields a significantly intensified and broadened absorption spectrum over a wide range, extending from the ultraviolet to the near-infrared region. Several factors contribute to this phenomenon, including the plasmonic behavior arising from the metallic content of ZrN/Zr_2ON_2,[9,36] the presence of oxygen/zirconium vacancies or interstitials[32,37] and a diverse distribution of particle sizes, as observed in Figure 2. Notably, the broad plasmon resonance spectrum featuring a central peak around 530 nm and the heightened light absorption within the visible-near infrared range at elevated temperatures hold immense promise for applications in solar light harvesting.

Figure 4 illustrates temperature measurements conducted within a metallic enclosure and on glass coated with ZrO_2 1150 nanoparticles. The temperature of the ZrO_2 1150-coated glass is depicted as the red trace, the air temperature within the chamber is represented by the black trace, and the photon flux is displayed as the blue trace (transmitted through a chamber window glass with over 90% light transmission). In Figure 4a, temperature measurements taken outdoors in an environment with an ambient air temperature of 26 °C are displayed for both inside the chamber and the glass film coated with ZrO_2 1150 nanoparticles, all under sunlight illumination.

The outcomes reveal a proportional increase in the temperature of the ZrO_2 1150-coated glass with rising photon flux. After a continuous 60-minute exposure to sunlight, the glass coated with ZrO_2 1150 nanoparticles reaches a peak temperature of 60 °C, presenting a temperature differential (ΔT) of approximately 15 °C above the air temperature within the enclosed metal box (around 45 °C). These initial findings strongly suggest the potential of zirconium oxynitride as a viable material for applications involving photothermal energy conversion.

https://doi.org/10.52111/qnjs.2023.17509

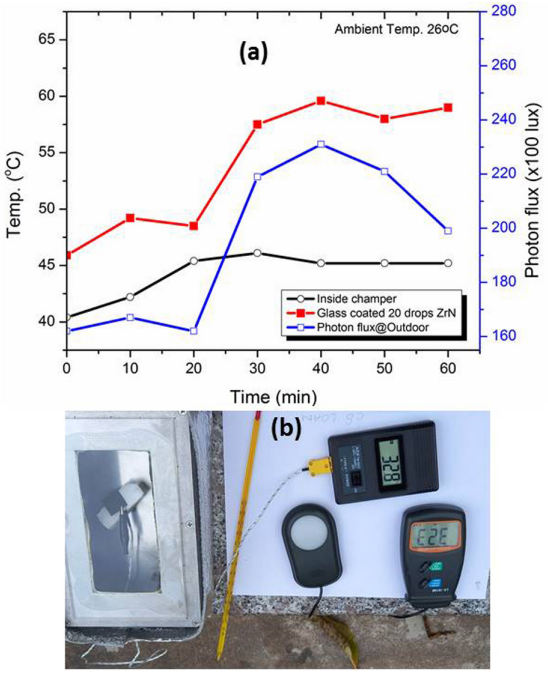

Figure 4. Temperature arising from ZrO_2 1150 material under sunlight exposure: the temperature of the ZrO_2 1150-coated glass is depicted as the red trace, the air temperature within the chamber is represented by the black trace, and the photon flux is displayed as the blue trace (transmitted through a chamber window glass with over 90% light transmission).

4. CONCLUSION

In brief, we have illustrated a straightforward method for producing zirconium(oxy)nitride nanoparticles. These particles display robust and extensive light absorption across a wide spectrum of solar wavelengths, encompassing the UV-vis to infrared range. We evaluated their ability for photothermal energy conversion by employing a metal chamber setup, where ZrO_2 1150 nanoparticles -coated glass were tested. The results indicated a significant heat generation, surpassing the surrounding temperature by approximately 30%. This experimentation underscores the promising prospects of utilizing zirconium(oxy)nitride for enhancing solar-to-heat conversion performance.

Acknowledgements

This work is financially supported by the Ministry of Education and Training of Vietnam under the grant number B2022-DQN-04.

REFERENCES

1. A. Lalisse, G. Tessier, J. Plain, and G. Baffou. Plasmonic efficiencies of nanoparticles made of metal nitrides (TiN, ZrN) compared with gold, *Scientific Reports*, **2016**, *6*, 1-10.
2. G. V. Naik, V. M. Shalaev, and A. Boltasseva. Alternative plasmonic materials: Beyond gold and silver, *Advanced Materials*, **2013**, *25*(24), 3264-3294.
3. P. Patsalas. Zirconium nitride : A viable candidate for photonics and plasmonics?, *Thin Solid Films*, **2019**, *688*, 137438.
4. B. J. Tan, Y. Xiao, F. S. Galasso, and S. L. Suib. Thermodynamic analysis and synthesis of zirconium nitride by thermal nitridation of sol-gel zirconium oxide, *Chemistry of Materials,* **1994**, *7*, 918-926.
5. U. Guler, V. M. Shalaev, and A. Boltasseva. Nanoparticle plasmonics: going practical with transition metal nitrides, *Materials Today*, **2015**, *18*(4), 1-11.
6. M. S. El-Eskandarany and A. H. Ashour. Mechanically induced gas-solid reaction for the synthesis of nanocrystalline ZrN powders and their subsequent consolidations, *Journal of Alloys and Compounds*, **2000**, *313*(1), 224-234.
7. Z. Wu, Z. Chen, L. Wang, L. Fang, T. Zhou, T. Mei, C. Zhang, Q. Li. Solid-state synthesis of zirconium nitride and hafnium nitride powders, *Journal of the Ceramic Society of Japan*, **2021**, *129*(3), 200-203.
8. S. Exarhos, A. Alvarez-Barragan, E. Aytan, A. A. Balandin, and L. Mangolini. Plasmonic core-shell zirconium nitride-silicon oxynitride nanoparticles, *ACS Energy Letters*, **2018**, *3*(10), 2349-2356.
9. R. A. Shishkin and E. S. Maiorova. Microwave vs autoclave synthesis of nanodisperse ZrN powder, *Glass and Ceramics*, **2017**, *74*(3), 123-125.
10. M. Banerjee, S. Kim, K. Xu, D. Barreca. Fabrication of ZrO_2 and ZrN films by metalorganic chemical vapor deposition employing new Zr precursors, *Crystal Growth & Design*, **2012**, *12*(10), 5079-5089.

11. A. S. Chernyavskii. Synthesis of ceramics based on titanium, zirconium, and hafnium nitrides, *Inorganic Materials*, **2019**, *55*(13), 1303-1327.

12. B. Fu and L. Gao. Synthesis of nanocrystalline zirconium nitride powders by reduction-nitridation of zirconium oxide, *Journal of the American Ceramic Society*, **2004**, *87*(4), 696-698.

13. B. J. Tan, Y. Xiao, F. S. Galasso, and S. L. Suib. Thermodynamic analysis and synthesis of zirconium nitride by thermal nitridation of sol-gel zirconium oxide, *Chemistry of Materials*, **1994**, *6*(7), 918–926.

14. S. K. Kim and V. V. Le. Surface & coatings technology cathodic arc plasma deposition of nano-multilayered ZrN/AlSiN thin films, *Surface and Coatings Technology*, **2011**, *206*(6), 1507–1510.

15. Z. Lei, Q. Zhang, X. Zhu, D. Ma, F. Ma, Z. Song, Y. Q. Fu. Corrosion performance of ZrN/ZrO_2 multilayer coatings deposited on 304 stainless steel using multi-arc ion plating, *Applied Surface Science*, **2018**, *431*, 170-176.

16. Y. Lu, Z. Yuan, H. Shen, X. Huai, and Z. Huang. High-temperature phase relations of ZrN–ZrO_2–Y_2O_3 ternary system, *Journal of Advanced Ceramics*, **2018**, *7*(4), 388-391.

17. T. Boldoo, J. Ham, E. Kim, and H. Cho. Review of the photothermal energy conversion performance of nanofluids, their applications, and recent advances, *Energies*, **2020**, *13*(21), 5748.

18. Y. Zhong, X. H. Xia, F. Shi, J. Y. Zhan, J. P. Tu, and H. J. Fan. Transition metal carbides and nitrides in energy storage and conversion, *Advanced Science*, **2016**, *3*(5), 1500286.

19. R. W. Harrison and W. E. Lee. Processing and properties of ZrC, ZrN and ZrCN ceramics: a review, *Advances in Applied Ceramics*, **2016**, *115*(5), 294-307.

20. N. Saiprasad, A. Boretti, L. Rosa. and S. Castelletto. Novel plasmonic materials to improve thin film solar cells efficiency, *Conference: Proc. SPIE 9668, Micro+Nano Materials, Devices, and Systems,* **2015**, 966847.

21. G. Baffou, F. Cichos, and R. Quidant. Applications and challenges of thermoplasmonics, *Nature Materials*, **2020**, *19* (9), 946-958.

22. L. T. T. Lieu, N. T. Lam, N. H. Hue, N. V. Nghia, N. M. Vuong, H. N. Hieu, N. V. Thang, L. V. Le, N. V. Huong, P.-C. Lin, A. Yadav, I. Madarevic, E. Janssens, H. V. Bui, and L. T. N. Loan. Titanium nitride nanodonuts synthesized from natural ilmenite ore as a novel and efficient thermoplasmonic material, *Nanomaterials*, **2021**, *11*(1), 76-87.

23. K. Xu, M. Du, L. Hao, J. Mi, Q. Yu, and S. Li. A Review of high-temperature selective absorbing coatings for solar thermal applications, *Journal of Materiomics*, **2020**, *6*(1), 167-182.

24. K. Ibrahim, H. Taha, M. M. Rahman, H. Kabir, and Z. T. Jiang. Solar selective performance of metal nitride/oxynitride based magnetron sputtered thin film coatings: A comprehensive review, *Journal of Optics (United Kingdom)*, **2018**, *20*(3), 033001.

25. P. R. Rauta, P. Manivasakan, V. Rajendran, B. B. Sahu, B. K. Panda, and P. Mohapatra. Phase transformation of ZrO_2 nanoparticles produced from zircon, *Phase Transitions*, **2012**, *85*(1), 13–26.

26. D. Manoharan, A. Loganathan, V. Kurapati, and V. J. Nesamony. Ultrasonics sonochemistry unique sharp photoluminescence of size-controlled sonochemically synthesized zirconia nanoparticles, *Ultrasonics Sonochemistry*, **2015**, *23*, 174–184.

27. J. C. Garcia, L. M. Scolfaro, A. T. Lino, V. N. Freire, and G. A. Farias. Structural , electronic, and optical properties of ZrO_2 from ab initio calculations, *Journal of Applied Physics*, **2006**, *100*, 104103.

28. P. Carvalho, J. M. Chappé, L. Cunha, S. Lanceros-Mendez, P. Alpuim, F. Vaz, E. Alves, C. Rousselot, J. P. Espinos, A. R. González-Elipe. Influence of the chemical and electronic structure on the electrical behavior of zirconium oxynitride films, *Journal of Applied Physics*, **2008**, *103*, 10.

29. W. Yin and Q. Wang. Feasibility of biological applications for zirconium nitride

https://doi.org/10.52111/qnjs.2023.17509

powders synthesized by gas – solid elemental combination method, *Journal of Nanoscience and Nanotechnology*, **2019**, *19*, 3319-3325.

30. L. Kumari, G. H. Du, W. Z. Li, R. S. Vennila, S. K. Saxena, and D. Z. Wang. Synthesis, microstructure and optical characterization of zirconium oxide nanostructures, *Ceramics International*, **2009**, *35*(6), 2401-2408.

31. A. Emeline, G. V. Kataeva, A. S. Litke, A. V. Rudakova, V. K. Ryabchuk, and N. Serpone. Spectroscopic and photoluminescence studies of a wide band gap insulating material: Powdered and colloidal ZrO_2 sols, *Langmuir*, **1998**, *14*(18), 5011-5022.

32. D. I. Bazhanov, A. A. Knizhnik, A. A. Safonov, A. A. Bagatur'yants, M. W. Stoker and A. A. Korkin. Structure and electronic properties of zirconium and hafnium nitrides and oxynitrides, *Journal of Applied Physics*, **2005**, *97*(4), 044108.

33. T. D. Boyko, A. Zerr, and A. Moewes. Tuning the electronic band gap of oxygen-bearing cubic zirconium nitride, *ACS Applied Electronic Materials*, **2021**, *3*, 4768-4773.

34. P. Carvalho, J. Borges, M. S. Rodrigues, N. P. Barradas, E. Alves, J. P. Espinós, A. R. González-Elipe, L. Cunha, L. Marques, M. I. Vasilevskiy, F. Vaz. Optical properties of zirconium oxynitride films: The effect of composition, electronic and crystalline structures, *Applied Surface Science*, **2015**, *358*, 660-669.

35. Q. Guo, T. Wang, Y. Ren, Y. Ran, C. Gao, H. Lu, Z. Jiang, and Z. Wang. Plasmonic properties of nonstoichiometric zirconium nitride, oxynitride thin films, and their bilayer structures, *Physical Review Materials*, **2021**, *5*(6), 65201.

36. L. Kumari, W. Z. Li, J. M. Xu, R. M. Leblanc, D. Z. Wang, Yi Li, Haizhong Guo, and Jiandi Zhang. Controlled hydrothermal synthesis of zirconium oxide nanostructures and their optical properties, *Crystal Growth & Design*, **2009**, *9*(9), 3874-3880.

37. S. Exarhos, A. A. Barragan, E. Aytan, A. A. Balandin, and L. Mangolini. Plasmonic core-shell zirconium nitride – silicon oxynitride nanoparticles, *ACS Energy Letters*, **2018**, *3*(10), 2349-2356.